Available online at www.sciencedirect.com
SCIENCE DIRECT
Polymer 46 (2005) 1331–1337
polymer
www.elsevier.com/locate/polymer

Silicone–polyacrylate composite latex particles. Particles formation and film properties

Mingtao Lin[a,b], Fuxiang Chu[a], Alain Guyot[b], Jean-Luc Putaux[c], Elodie Bourgeat-Lami[b,*]

[a]*Institute of Chemical Products of Forestry, Sinica Academy of Forestry, 210042 Nanjing, China*
[b]*Laboratoire de Chimie et Procédés de Polymérisation, UMR 140 CNRS-CPE-Lyon, BP 2077, 69616 Villeurbanne, France*
[c]*Centre de Recherche sur les Macromolécules Végétales, UPR 5301 CNRS, BP 53, F-38041 Grenoble Cedex 9, France*

Accepted 30 September 2004

Abstract

Composite latex particles with a polydimethylsiloxane PDMS core and a poly(methyl methacrylate-*co*-*n*-butyl acrylate) P(MMA-BA) copolymer shell were synthesized by seeded emulsion polymerization using the PDMS latex as the seed. The compatibility between the two polymer phases was changed by introducing vinyl groups in the latex core. Monomer conversions and particle size evolution were monitored to see the influence of the nature of the core functionality on the polymerization kinetics and on the extent of secondary nucleation. Particle morphology was characterized by cryo-transmission electron microscopy. The P(MMA-BA) copolymer formed a regular shell around the PDMS seed, whereas nonuniform coatings were formed when vinyl functionalities were introduced into the seed. Films were produced from the latexes, and their surface property was analyzed by X-ray photoelectron spectroscopy and contact angle measurements. It was shown that the PDMS component segregated to the polymer/air interface and that the extent of segregation depended on the original particles structure. Because PDMS has a very low glass transition temperature, it can easily diffuse throughout the film material. However, protected by an acrylic shell, polymer diffusion is significantly hindered and the film then displays all the characteristic properties of the acrylic copolymer. The surface composition of the films formed by the structured particles which PDMS core was not totally covered by the polyacrylate, was found to be intermediate between the composition of the films issued from the core–shell latexes and that of the films produced from blends of pure polyacrylate and PDMS latexes.

Keywords: Polydimethylsiloxane; Polyacrylate; Seeded emulsion polymerization

1. Introduction

Silicone polymers are of high scientific and technological interest owing to their unique characteristics such as high flexibility, excellent thermal stability, high gas permeability and low surface energy. Their utilization is, however, limited due to their poor mechanical properties. It thus appears of interest to incorporate polysiloxane polymers into film-forming polyacrylic lattices to take advantage of the properties of the polydimethylsiloxane (PDMS) homopolymers (e.g. the water repellency and the emmoliency of the silicone polymer), as well as of the mechanical strength and cohesiveness of the acrylic matrix. Most of the works in this field are in the patent literature [1–3] and only a few papers describe the synthesis of such materials in the open literature [4–13]. Since the properties of the resulting film materials are expected to be influenced by the original particles morphology, much effort has been devoted so far to produce composite particles with controlled shapes and compositions. Core–shell particles with a silicone core and an acrylic copolymer shell were produced for instance by seeded emulsion polymerization of acrylic monomers in the presence of various siloxane polymer latexes [4–7]. Similarly, Kong and co-authors have reported on the synthesis of polyacrylate–silicone core–shell particles using hydrophilic acrylic monomers in a first stage and siloxanes in a second stage of the seeded emulsion polymerization process [8,9]. Owing to the different properties of the core and shell materials, the incorporation

* Corresponding author. Tel.: +33 72 43 17 77; fax: +33 472 43 17 68.
E-mail address: bourgeat@lcpp.cpe.fr (E. Bourgeat-Lami).

0032-3861/$ - see front matter © 2004 Elsevier Ltd. All rights reserved.
doi:10.1016/j.polymer.2004.11.063

of functional monomers on the seed surface appeared a key feature in order to achieve the desired morphology. An alternative strategy consists in performing the radical and the ionic ring-opening polymerization simultaneously in order to produce hybrid copolymer latexes with interpenetrated silicone–polyacrylate networks [10–13]. Functional monomers like tetramethyl tetravinyl cyclo tetrasiloxane or methacryloxy propyl trimethoxysilane were again used in order to create covalent bonds between the polysiloxane and the polyacrylate and prevent phase separation [10–13].

In this paper, we report results along this line on the synthesis of silicone/polyacrylate composite latexes through seeded emulsion polymerization of acrylic monomers in the presence of PDMS latexes. The principal objective of this work is to investigate the impact of the original particles morphology on the properties of the films obtained from the latexes since particles with tailored morphology are expected to give properties which are not accessible by simply physically blending of the polymeric components. In particular, we can expect a better compatibility and a more regular distribution of the two phases within the film material without the occurrence of significant phase segregation.

In order the check the influence of the properties of the seed particles on the seeded growth process, a series of PDMS samples were prepared by cationic miniemulsion polymerization and compared to a polyacrylate latex seed. Cryo-transmission electron microscopy (cryo-TEM), differential scanning calorimetry (DSC) and X-ray photoelectron spectroscopy (XPS) were used to characterize the morphology of the composite particles as well as the surface properties of the hybrid films produced from the latexes. Wettability and solubility measurements were additionally performed on the films and compared to pure polyacrylate or to mixtures of PDMS and polyacrylate.

2. Experimental section

2.1. Materials

Methyl methacrylate (MMA, Acros) and *n*-butyl acrylate (BA, Acros) were used as received. Dodecylbenzenesulfonic acid sodium salt (SDBS, Fluka), dodecylbenzene sulfonic acid (DBSA, Acros) and ammonium persulfate (APS, Acros) were used without further purification. Octamethyl cyclo tetrasiloxane (D_4, Acros) and tetramethyl tetravinyl cyclo tetrasiloxane (D_4^V, Aldrich) were used as supplied. Deionized water was used to prepare all the solutions and emulsions.

2.2. Polymerization procedures

2.2.1. Synthesis of the seed latex particles

The PDMS and P(D_4–D_4^V) seed latexes were synthesized in miniemulsion by cationic ring-opening polymerization of D_4 or a mixture of D_4 and D_4^V following a procedure described previously [14]. The recipes are given in Table 1. For comparison purposes, a latex (denoted PA) with the same composition as the shell polymer was synthesized in miniemulsion using the recipe given in Table 1.

2.2.2. Seeded growth polymerization

The seed latex (30 g) and water (95 g) were poured into the reactor. The mixture was purged with nitrogen for 15 min. Then, the appropriate amount of APS (0.2 g), dissolved into 5 g of water, was introduced into the reactor and the monomer mixture (MMA (10 g) and BA (10 g)) was added dropwise in the suspension medium at the rate of 5 ml h^{-1} at 70 °C under a nitrogen atmosphere for up to 6 h. The resulting composite samples were called PA@PA, PDMS@PA and P(D_4–D_4^V)@PA, respectively.

2.3. Characterization methods

2.3.1. Particle size measurement

Particles size were determined by dynamic light scattering (DLS) using a Malvern autosizer Lo-c apparatus with a detection angle of 90°. The measurements were carried at 23 °C on highly diluted samples in order to rule out interaction and multiple scattering effects. The intensity average diameter was computed from the intensity autocorrelation data using the cumulant analysis method [15].

2.3.2. Surfactant adsorption measurements

The PDMS and P(D_4–D_4^V) latexes were coagulated by dropwise addition of a 0.1 M $CaCl_2$ water solution. The water phase was then separated by filtration and the surfactant concentration was determined by UV spectroscopy using calibration curves. The UV analysis was performed using an UV/VIS spectrophotometer (UVIKON 922) and quartz cells. The measurements were carried out at wavelengths of 195 nm ($\varepsilon = 35{,}305$ mol l^{-1}) or 225 nm ($\varepsilon = 10{,}788$ mol l^{-1}) for both the SDBS and DBSA

Table 1
Recipes for the synthesis of the seed latexes by miniemulsion polymerization

Seed	MMA	BA	HD[a]	SDBS	APS	H_2O	DBSA	D_4	D_4^V
PA	25	25	1	0.6	0.5	250	/	/	/
PDMS	/	/	/	0.3	/	125	0.8	25	/
P(D_4–D_4^V)	/	/	/	0.3	/	125	0.8	22.5	2.5

[a] Hexadecane. All the data are indicated in grams.

surfactants. The amount of adsorbed surfactant was determined by difference between the total amount and the free amount of surfactant.

2.3.3. Cryo-TEM

According to procedures described elsewhere [16–18], specimens for cryo-TEM were prepared by fast-freezing thin films of particle suspensions diluted to a concentration of about 1 mg ml^{-1}. The samples were then mounted in a Gatan 626 specimen holder cooled down with liquid nitrogen, transferred in a Philips CM200 'Cryo' microscope and observed under low dose illumination, at −180 °C. Micrographs were recorded on Kodak SO163 films.

2.3.4. Film formation

Films were prepared at 60 °C by casting either the PDMS@PA or the P(D_4–D_4^V)@PA latex suspensions in an aluminum mold and drying for 24 h. Films were also produced from physical blends of PDMS or vinyl-functionalized PDMS with the polyacrylate copolymer, and will be denoted in the following as PDMS + PA and P(D_4–D_4^V) + PA, respectively.

2.3.5. DSC analysis

Appropriate amounts of samples were sealed in aluminum sample pans and were prepared by compression molding. DSC thermo-scans of the hybrid materials were then recorded under a dry nitrogen atmosphere at a heating rate of 10 °C min^{-1} from −145 to 150 °C, in two scans using a Setaram DSC 131 apparatus.

2.3.6. Contact angle and XPS measurements

Surface tension determination. Contact angle measurements were performed on a GBX-Instrumentation Digidrop apparatus at 25 °C using the drop method [19]. A 5 μl liquid drop was deposited onto the surface of the hybrid film using a micrometer syringe fitted with a stainless steel needle. The contact angle on both sides of the drop was measured to ensure symmetry. The probes used for contact angle determination were water, formamide ($HCONH_2$) and bromonaphtalene ($C_{10}H_7Br$). The surface energy (i.e. the sum of the polar energy and dispersive energy) of the different film materials was determined using the Fowkes–Kaelble method using Eq. (1) below [20]:

$$(1 + \cos\theta)\gamma_L = 2[(\gamma_L^d\gamma_s^d)^{0.5} + (\gamma_L^p\gamma_s^p)0.5] \quad (1)$$

where θ is the equilibrium contact angle of the liquid (L) on the solid surface (S), γ_L and γ_S are the surface tensions of liquid and solid, respectively, and γ_L^p, γ_L^d, γ_S^p, γ_S^d are the polar and dispersive components of the liquid and solid surface tensions, respectively.

$$\gamma_L = \gamma_L^d + \gamma_L^p \text{ and } \gamma_S = \gamma_S^d + \gamma_S^p \quad (2)$$

Eq. (1) thus allows us to estimate γ_S via measurement of the contact angles of two liquids for which we know the values of γ_L, γ_L^d and γ_L^p.

XPS analysis. XPS spectra were recorded using a VG ESCALAB MK apparatus. The surface composition (in at.%) of the various PDMS, PDMS@PA and P(D_4–D_4^V)@PA samples was determined by considering the integrated peak area of the Si(2p): 106 eV, C(1s): 289 eV and O(1s): 536 eV and their respective sensitivity factors.

2.3.7. Infrared analysis

The Fourier Transform Infra-Red (FTIR) spectra were recorded on powder pressed KBr pellets using a Nicolet 460 spectrometer with a resolution of 4 cm^{-1}.

3. Results and discussion

3.1. Latex seeds synthesis

All the latex seeds were prepared in miniemulsion using recipes shown in Table 1. The polyacrylic latex was synthesized by free radical polymerization using APS as initiator, SDBS as anionic surfactant and hexadecane as the hydrophobe, whereas the polysiloxane seeds were prepared by cationic ring-opening polymerization of the cyclosiloxane. The latexes had a solid content of 16.7% and particle size comprised between 150 and 190 nm. The PDMS and P(D_4–D_4^V) number average molecular weights were found to be around 110,500 g mol^{-1}.

3.2. Seeded emulsion polymerization

In order to understand the effect of the chemical nature of the latex core on kinetics and morphology, particle size and monomer conversions were followed as a function of time for a series of seeded emulsion polymerization performed using the lattices described above. These experiments were performed at a fixed surfactant concentration and a fixed weight ratio between the first and second stage polymers.

Using a PA seed leads to a very classical emulsion polymerization. As shown in Fig. 1, the polymerization rate

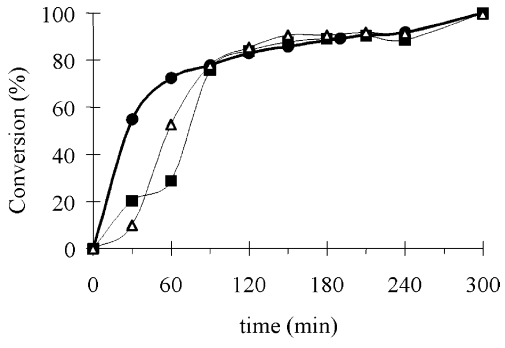

Fig. 1. Evolution of conversion as a function of time during the seeded emulsion polymerization of MMA and BA using P(MMA-BA) (●), PDMS (■) and P(D_4–D_4^V) (△) latexes as the seeds.

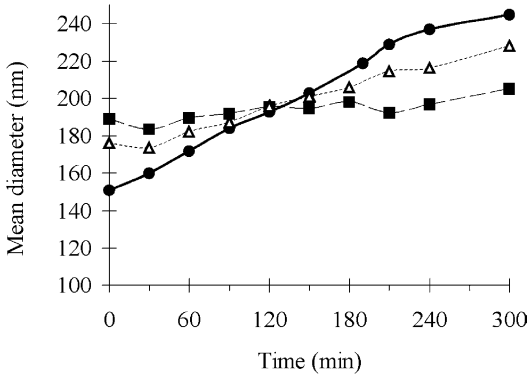

Fig. 2. Evolution of particles size as a function of time during the seeded emulsion polymerization of MMA and BA using P(MMA-BA) (●), PDMS (■) and P(D_4–D_4^V) (△) latexes as the seeds.

is high without any induction period and progressively decreases as the reaction time increases. On the other hand, the particles diameter increases while the particles number remains constant (see Figs. 2 and 3). In contrast, the polymerization performed using a PDMS seed exhibits a first induction period followed by a second induction period characterized by a decrease in the polymerization rate. A high conversion is finally reached upon increasing the reaction time while renucleation concurrently takes place: the particle size remains almost constant while the particle number progressively increases as shown in Figs. 2 and 3, respectively.

The polymerization performed using the P(D_4–D_4^V) seed shows a very similar behavior. After an induction period of around 30 min, the reaction rate progressively increases and then decreases at higher conversions. Renucleation still occurs as in the case of the PDMS seed but to a lesser extent. The particle number increases by a factor 2 instead of a factor 4 in the previous case.

Since the presence of extra surfactant might be at the origin of the formation of a secondary particle population, the surfactant distribution of the original seed latexes was monitored by surfactant adsorption measurements. The results show that, in every case, the free surfactant

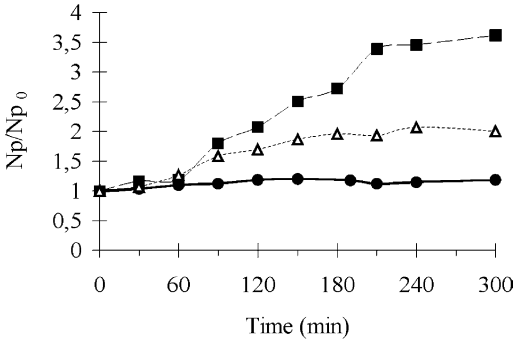

Fig. 3. Evolution of the ratio, N_p/N_{p_0}, of the number of composite particles over the number of seed particles as a function of time during the seeded emulsion polymerization of MMA and BA using P(MMA-BA) (●), PDMS (■) and P(D_4–D_4^V) (△) latexes as the seeds.

concentration in the water phase is lower than the critical micellar concentration (CMC) of the soap. Secondary nucleation in systems below the CMC is thought to occur by homogeneous nucleation: z-mers in the aqueous phase propagate to higher chain lengths (instead of entering a preexisting particle) until they reach a critical degree of polymerization j_{crit}, whereupon they become insoluble and form precursor particles that grow into latex particles [21, 22]. Owing to the substantial difference in polarity of the PDMS and PA domains and the high water solubility of the acrylic monomer mixture, the polymerization is expected to preferentially take place in the water phase. The resulting primary particles are then presumed to aggregate onto the seed surface to form the shell layer. In the case of vinyl-functionalized PDMS seed, it can be suggested that the double bond of D_4^V undergoes a copolymerization with the acrylic monomers so that grafting can also take place. Anchoring of the precipitating oligomers on the seed surface in the early stages of the emulsion polymerization process may consequently promote the formation of a PA overlayer and decrease the probability of secondary nucleation.

3.3. Composite particles morphology

Fig. 4a shows spherical composite particles formed using the PDMS seed. At first approximation, two families of particles seem to be observed. The larger particles, whose diameter (170–200 nm) is in good agreement with the DLS data, exhibit a clear core–shell morphology. A more or less clearly defined dark spherical core can be seen when the particle is not too large. It likely corresponds to the PDMS seed surrounded by a PA shell of lower density (Fig. 4a). There appears to be a second family of particles with a diameter of 70–80 nm although their proportion was difficult to estimate reliably from the images. These smaller particles do not exhibit a very dark core like the larger ones and may correspond to the secondary population of particles mentioned above. However, a careful examination of the images suggests that some of them may also contain a seed.

The composite particles prepared with the P(D_4–D_4^V) seed have a clearly different and more complex morphology (Fig. 4b). They are generally multilobular, most particles exhibiting three lobes surrounding a darker core and an average diameter of 200–230 nm. A number of smaller particles only have two lobes but the darker core can still be seen. Some 100–120 nm spherical particles can also be seen that may correspond again to the secondary crop of polyacrylate particles produced during the seeded-growth process. By analogy with the different contrasts observed on the PDMS-seeded core–shell particles, the dark central part of the multilobular particles must correspond to the P(D_4–D_4^V) seed. However, its topology is completely different from that of the spherical PDMS seed. Surprisingly, it seems to be deformed, adjusting to the interspace defined by the constituting PA lobes. Although it is difficult to determine quantitatively the degree of surface coverage and the

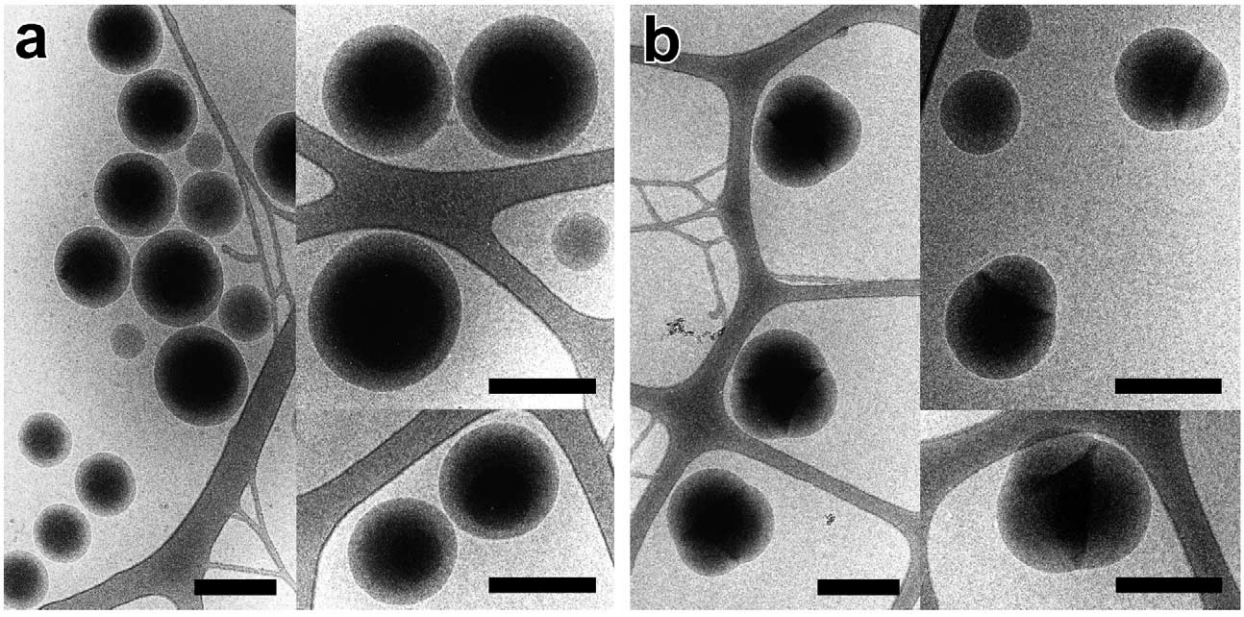

Fig. 4. Cryo-TEM micrographs of silicone/polyacrylate composite particles synthesized by seeded emulsion polymerization of MMA and BA using two different seeds: (a) PDMS. On the right, images at a higher magnification where the darker seeds are seen more clearly inside the particles (scale bars: 200 nm); (b) P(D_4–D_4^V). On the right, images at a higher magnification showing particles with two or three constituting lobes. The darker area corresponds to the P(D_4–D_4^V) core (scale bars: 200 nm).

thickness of the interface between the P(D_4–D_4^V) core and the PA domains, it clearly appears from the TEM pictures that the polysiloxane is not totally covered by the acrylic copolymer. It may be suggested that the PDMS seed has a glass transition temperature (T_g) much lower than that of PA, and can be easily deformed upon the formation of cross-links by reaction of D_4^V with MMA and BuA. Moreover, it is worth to notice that cross-linking may also promote the phase separation between the seed polymer and the secondary polymer by restricting the diffusion of the oligomeric radical and preventing phase rearrangements.

In order to confirm the occurrence of grafting between the polyacrylate and polysiloxane, we carried out Soxhlet extraction experiments of the latex films with THF. While the PDMS and PDMS@PA latex films were found to be totally soluble in boiling THF, the P(D_4–D_4^V)@PA sample was only partially soluble giving clear evidence of cross-linking. The FTIR spectrum of the insoluble fraction shows signals characteristics of both the PDMS and the polyacrylate phases (see Supporting information), indicating that cross-linking occurred by copolymerization reaction of MMA and BuA monomers with the pendant vinyl groups of the P(D_4–D_4^V) copolymer as suspected.

3.4. Macroscopic film properties

As far as applications are concerned, it is essential to determine to what extent film properties are influenced by the above reported morphologies.

3.5. DSC analysis

It is well known that PDMS displays a T_g at around −123 °C and exhibits at higher temperature phase transition phenomena, i.e. crystallization (T_c) and melting (T_m). In Fig. 5, the thermal behavior of PDMS is compared to that of: (1) the PA matrix, (2) blends of PDMS or P(D_4–D_4^V) with PA, and (3) the PDMS@PA or the P(D_4–D_4^V)@PA composite latexes. The data are reported in Table 2.

Owing to the sensitivity of the DSC method and considering the low PDMS content of the samples, all the composite materials revealed only one T_g at around 18 °C corresponding to the PA matrix. The latex blends showed, in

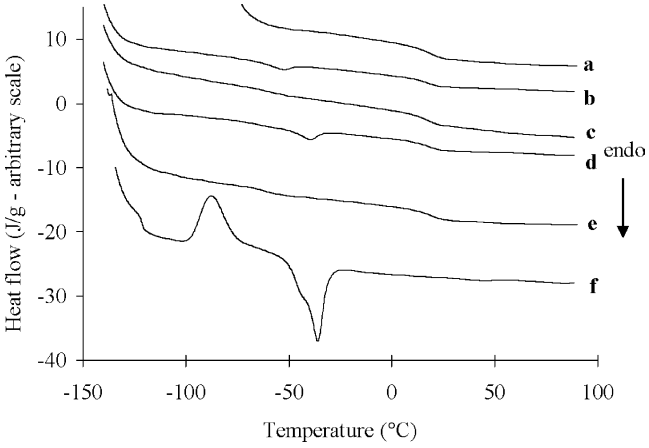

Fig. 5. DSC thermogram* of the different film materials: (a) PA, (b) PDMS + PA, (c) PDMS@PA, (d) P(D_4–D_4^V) + PA, (e) P(D_4–D_4^V)@PA and (f) PDMS. *The thermograms have been shifted vertically for clarity.

Table 2
DSC analysis of the hybrid film materials

	T_g (°C)			T_c (°C)			T_m (°C)		
	T_{g_i}	T_g	T_{g_f}	T_{c_i}	T_c	T_{c_f}	T_{m_i}	T_m	T_{m_f}
PA	12.0	18.7	25.4	/	/	/	/	/	/
PDMS	−122.4	−121.3	−120.3	−93.3	−87.6	−82.2	−37.7	−35.8	−30.7
PDMS+PA	11.1	18.0	23.5	/	/	/	−42.3	−39.6	−36.9
PDMS@PA	12.7	17.8	21.9	/	/	/	/	/	/
$P(D_4–D_4^V)$	−123.0	−122.1	−121.2	−95.9	−89.8	−77.7	−56.1	−50.6	−47.9
$P(D_4–D_4^V)$+PA	12.9	17.3	22.8	/	/	/	−58.0	−52.7	−50.0
$P(D_4–D_4^V)$@PA	11.9	17.3	22.8	/	/	/	/	/	/

Data not available.

addition to a T_g, a melting endotherm with a maximum at −39.6 and −52.7 °C, respectively. A decrease in the melting temperatures of the latex blends compared to pure PDMS or $P(D_4–D_4^V)$ can be noticed, whose effect is consistent with a decrease in the size of the crystalline domains.

In addition, such a phase transition phenomenon could not be detected at all in either the PDMS@PA or the $P(D_4–D_4^V)$@PA composite samples suggesting in this case a significant reduction of the amount of PDMS that could form a crystalline phase.

3.6. Contact angle measurement and XPS analysis

Different methods are available to estimate the surface energy of solid materials (γ_S). One method consists in measuring the contact angle between the solid and different liquids and applying Eq. (1) as reported in Section 2. Table 3 shows the results of this analysis for different couples of liquids.

The surface tension of the hybrid films illustrates the surface properties of the different materials. As expected, PDMS has a low surface energy compared to PA. The surface energy of either the PDMS+PA or the $P(D_4–D_4^V)$+PA latex blends is close to that of pure PDMS suggesting that the siloxane polymer chains had moved on the surface in order to lower the interfacial tension of the films. However, this effect is less pronounced for the latex blends based on $P(D_4–D_4^V)$ than for those based on PDMS. It is likely that the mobility of the PDMS domains is reduced in the former case because of cross-linking reactions occurring during film formation. Indeed, such reactions are expected to significantly hinder the possible migration of the PDMS chains within the film material. The mobility of the siloxane polymers also appeared to be drastically influenced by the formation of a regular and protecting PA shell around the PDMS latex core as indicated by the high surface tension of the PDMS@PA latex films. Such a result definitely supports the assumption of formation of a PA-rich surface and is in perfect agreement with the previous TEM observations of the individual composite particles. Finally, the surface tension of the $PD_4D_4^V$@PA composite materials is similar to that of the corresponding $P(D_4–D_4^V)$+PA latex blend and lower than the surface energy of the PDMS@PA film material. Since in this case, the PA does not completely cover the PDMS core, the final properties of the composite film are not dominated by the characteristics of PA but are intermediate between that of PA and that of PDMS, a result which is again consistent with cryo-TEM observations of the individual latex particles.

Complementary information on the elemental composition of the film surface was provided by XPS analysis. This technique is well documented in the literature and provides insights into the stoichiometry of the surface. The XPS surface composition of the different film materials are reported in Table 4.

At first approximation, the XPS data seem to be in contradiction with the contact angle measurements. Indeed, the surface composition of the PDMS@PA film sample are more silicon-rich than its corresponding bulk composition indicating that the stoichiometry of the sub-surface region is dominated by the PDMS component. The predominance of

Table 3
Experimental values of the surface tension of the different film materials determined from contact angle measurements with a series of wetting liquids

Series	Surface tension: γ_s (10^{-3} N m^{-1})			
	H_2O/$HCONH_2$	H_2O/$C_{10}H_7Br$	$HCONH_2$/$C_{10}H_7Br$	Average
PA	64.1	40.9	51.5	52.2
PDMS	13.6	20.4	29.0	21
PDMS+PA	17.8	25.5	24.3	22.5
PDMS@PA	63.6	28.9	46.7	46.4
$P(D_4–D_4^V)$	14.4	25.2	25.5	21.7
$P(D_4–D_4^V)$+PA	39.1	24.8	31.0	31.6
$PD_4D_4^V$@PA	39.7	38.9	40.4	39.7

Table 4
XPS surface compositions (at.%) of the PDMS and the PDMS–polyacrylate composite film materials. The values in brackets correspond to the bulk compositions

	Si	C	O
PDMS	24.06 (25.0)	50.24 (50.0)	25.69 (25.0)
PDMS@PA	18.66 (3.3)	53.22 (71.3)	28.12 (25.3)
$P(D_4–D_4^V)$@PA	5.59 (2.8)	71.44 (72.5)	22.97 (24.6)

The values in brackets correspond to the bulk compositions.

the silicon atom signal in the XPS spectrum may be due to the low PA shell thickness compared to the photoelectron penetration depth (3–5 nm). In contrast, the composition of the $P(D_4–D_4^V)$@PA latex film is close to the theoretical one, indicating a random distribution of the PDMS and PA phases within the composite film material. In this case, it is likely that some PDMS diffuses out of the particles during film formation and redistribute in the composite film material. The apparent discrepancy between the contact angle and XPS measurements can be thus ascribed to instrumental differences in probing depths. While contact angle measurements enable to characterize the top layer surface properties of the latex film, XPS probes deeper inside the film structure and provides information on the sub-layer structure.

4. Conclusions

Composite latexes with a soft polysiloxane core surrounded by a film forming P(MMA-BA) copolymer were prepared by seeded emulsion polymerization using a variety of polysiloxane latexes as the seeds. The seeds were produced by miniemulsion polymerization and displayed different particle size. Some of the most important results found were as follows. Core–shell particles were obtained when the seeded emulsion polymerization process was carried out with dropwise addition of the monomers in the presence of a pure PDMS seed. When reactive vinyl functionalities were introduced in the latex core, particles with uneven surfaces were produced. Anchoring of the growing polymeric radicals to the PDMS core and the formation of cross-links promoted the deformation of the latex seed with a drastic impact on the final particle morphology. The combination of various techniques such as cryo-TEM, XPS, contact angle and FTIR analysis enabled us to find reliable correlations between the individual particle structure and the surface characteristics of the dispersion films. It was found that in case of the core–shell particles, the oily hydrophobic PDMS was embedded into a matrix of the more hydrophilic second stage acrylic copolymer, in agreement with the hypothesis of the formation of a closed and protective polyacrylic shell. In contrast, the film surface generated from the multilobular particles showed a higher degree of hydrophobicity as a result of incomplete shell formation and possible migration of the internal PDMS domains in-between the polyacrylic hemispheres. The later assumptions might be confirmed by further morphological characterizations of the hybrid films using for instance atomic force microscopy (AFM).

Acknowledgements

The authors thank the French/Chinese association for its financial support.

Supplementary data

Supplementary data associated with this article can be found, in the online version, at doi:10.1016/j.polymer.2004.11.063.

References

[1] Shimozawa S, Koshio T. Japan Patent 03-227312; 1991.
[2] Olson KG, Hartman ME, Das SK, Dowbenko R. European Patent Application 0153600; 1985.
[3] (a) Burzynski AJ, Martin RE. US Patent 3449293; 1969.(b) Thomas RN. US Patent 3575910; 1971.(c) Hilliard JR. US Patent 3898300; 1975.
[4] Kong XZ, Ruckenstein E. J Appl Polym Sci 1999;73:2235.
[5] (a) He WD, Cao CT, Pan CY. Polym Int 1996;39:31.
(b) He WD, Cao CT, Pan CY. J Appl Polym Sci 1996;61:383.
(c) He WD, Pan CY. J Appl Polym Sci 2001;80:2752.
[6] Okaniwa M. Polymer 2000;41:453.
[7] Dai Q, Zhang Z, Wang F, Liu J. J Appl Polym Sci 2003;88:2732.
[8] Kong XZ, Kan CY, Yuan Q. Polym Adv Tech 1996;7:888.
[9] Kan CY, Kong XZ, Yuan Q, Liu DS. J Appl Polym Sci 2001;80:2251.
[10] Kan CY, Liu DS, Kong XZ, Zhu XL. J Appl Polym Sci 2001;82:3194.
[11] Kan C, Yuan Q, Wang M, Kong X. Polym Adv Tech 1996;7:95.
[12] Kan CY, Zhu XL, Yuan Q, Kong XZ. Polym Adv Tech 1997;8:631.
[13] Wu YM, Duan HD, Yu YQ, Zhang CG. J Appl Polym Sci 2000;79:333.
[14] Lin M, Chu F, Bourgeat-Lami E, Guyot A. J Disp Sci Technol 2004;25:827.
[15] Koppel DJ. Chem Phys 1972;57:4814.
[16] Harris JR. In Negative staining and cryoelectron microscopy. Oxford: Bios Scientific Publishers; 1997.
[17] Durrieu V, Putaux JL, Passas R, Gandini A. Microsc Anal (Eur ed) 2004;18:5.
[18] Chalaye S, Bourgeat-Lami E, Putaux JL, Lang J. Macromol Symp 2001;169:89.
[19] Kaelble DH. Phys chem of adhesion. New York: Wiley Interscience; 1971.
[20] Toussaint AF, Luner P. Contact angle, wettability and adhesion. In: Mittal KL, editor, 2003, p. 383–96.
[21] Hansen FK, Ugelstad J. In: Piirma emulsion polymerization. New York: Academic Press; 1982.
[22] Fitch RM. ACS Symp Ser 1981;165:1. Fitch RM. Br Polym J 1973;5:467.